

University of Nevada, Reno

Microstructure Nanocomposites for Thermoelectrics

A thesis submitted in partial fulfillment of the
requirements for the degree of Master of Science in
Mechanical Engineering

by

Connor Richard Rock

Dr. Yan Wang/Thesis Advisor

May 2019

© by Connor Richard Rock 2019

All Rights Reserved



THE GRADUATE SCHOOL

We recommend that the thesis
prepared under our supervision by

Entitled

be accepted in partial fulfillment of the
requirements for the degree of

, Advisor

, Committee Member

, Graduate School Representative

David W. Zeh, Ph.D., Dean, Graduate School

ABSTRACT

According to the Lawrence Livermore National Laboratory, nearly 70% of energy produced in the United States was wasted in the form of heat in 2018 [3]. With this ongoing energy crisis and increasing energy demands, there lies an urgent need for improved energy harnessing materials. Thermoelectric (TE) materials can convert a temperature gradient into an electric potential or vice versa. The efficiency of these materials is characterized using a dimensionless figure of merit (ZT). In order for these materials to become economically feasible, the ZT values need to be significantly increased from their current standing. Nanostructuring of these materials is a plausible option that can significantly increase ZT . In this study, we seek to demonstrate through classical molecular dynamic simulations and experimental investigations how the nanostructuring of particle size in $\text{Ge}_2\text{Sb}_2\text{Te}_5$ nanocomposites can reduce the lattice thermal conductivity, and in turn, increase the figure of merit of TE materials.

ACKNOWLEDGEMENTS

I would like to thank my advisor, Dr. Yan Wang, for his continued encouragement and support in research opportunities at the University of Nevada, Reno. His guidance and expertise have directed me throughout the entire process of research and of writing my thesis. He serves as an inspiration to me and my aspirations to be a professional who continues to engage in lifelong learning. I would also like to thank Dr. Lei Cao, and Dr. Samuel Odoh, who have also supported my research efforts throughout my studies. They are terrific examples of experts in their field of study and as leaders at the University of Nevada.

Additionally, I would like to thank Patrice Kusnierczyk. The steadfast love and encouragement I have received from her has inspired me to become the best person I can be. Her selfless care and determined attitude inspire everyone she meets to be their best self.

Finally, I would like to thank my friends and family. Namely, I would like to thank my father, mother, brother, and grandparents for their unwavering love and support throughout my educational career. They have inspired me to achieve my dreams.

We acknowledge the financial support from the NASA EPSCoR program (NASA Space Grant NNX15AK48A).

TABLE OF CONTENTS

LIST OF TABLES.....	iv
LIST OF FIGURES.....	v
1. INTRODUCTION TO THERMOELECTRIC MATERIALS.....	1
1.1. Principles of Thermoelectrics.....	1
1.2. Lattice Thermal Transport.....	4
2. THERMOELECTRIC MATERIALS.....	5
2.1. Half-Heuslers.....	7
2.2. Skutterudites.....	8
2.3. Bi_2Te_3	10
2.4. $\text{Ge}_2\text{Sb}_2\text{Te}_5$	11
2.5. Nanoparticle Size Distribution.....	13
3. EXPERIMENTAL and SIMULATION INVESTIGATION.....	16
3.1. Background and Motivation.....	16
3.2. Molecular Dynamic Simulation of Thermal Transport in Polycrystals....	17
3.3. Experimental Investigation of Thermal Transport in Polycrystalline $\text{Ge}_2\text{Sb}_2\text{Te}_5$	20
3.3.1. $\text{Ge}_2\text{Sb}_2\text{Te}_5$ Sample Preparation.....	20
3.3.2. Experimental Procedure.....	22
4. RESULTS AND DISCUSSION.....	24
4.1. Results of Molecular Dynamic Simulations.....	24
4.2. Results of Thermal Conductivity Measurements.....	26
4.2.1. SEM Analysis.....	28
4.3. Discussion of Results and Experimental Errors.....	31
4.3.1. Discussion.....	31
4.3.2. Experimental Errors.....	32
5. CONCLUSION AND FUTURE WORK.....	34
5.1. Conclusion.....	34
5.2. Future Work.....	35
REFERENCES.....	37

LIST OF TABLES

Table

1. Ge ₂ Sb ₂ Te ₅ sample fabrication parameters.....	22
2. Comparison of the simulation results for thermal conductivity of solid argon with varying number of grains per structure.....	25
3. Average thermal conductivity and standard deviations of the GST samples as measured by the LFA.....	27

LIST OF FIGURES

Figure

1. Diagram of thermoelectric generator and working mechanisms.....1
2. Different phonon scattering mechanisms utilized by materials to reduce the lattice thermal conductivity.....6
3. Unit cell of CoSb_3 skutterudite. Co occupies 'c' sites, Sb occupies 'g' sites, and filler atoms may occupy the 'a' site.....9
4. Unit cell structure of the a) crystalline phase, b) melt quenched glass, c) ideal glass of $\text{Ge}_2\text{Sb}_2\text{Te}_5$12
5. General methods of improving phonon scattering through structure modification [21]. Represented above are e) micrometer grains, f) nanometer grains, g) mixture of different sized grains, h) mixture of nanoparticles with a variety of compositions, i) compaction of a mixture of two components, j) nanosize precipitates within bulk material.....15
6. The simulated structures generated by AtomsK containing a) 4 grains b) 8 grains c) 16 grains and d) 32 grains [23]. The green, white, and red spheres represent FCC, amorphous, and HCP structure types, respectively. Note that the structure in panels a-d seem to have more than the designated number of grains, which is merely a result of the periodic boundary condition used in OVITO.....19
7. Images of GST powder before grinding and ball milling process (left) and fabricated pellet (GST-4) as a result of the cold sintering press (right).....21
8. Schematic of components of LFA 447.....23
9. Grain size dependence of the thermal conductivity of solid argon at 30 K over 10000 time steps. The average thermal conductivity of single-crystalline sample is 73.4 W/mK, as predicted by our molecular dynamic simulations.....26
10. Average bulk thermal conductivity measurements of GST samples.....27
11. SEM surface micrographs of a) location 1 and b) location 2 on a 12-hour milled sample.....28
12. Location used for EDS analysis containing area indicated in Fig. 11b.....30

13. EDS analysis of micrograph in Fig. 12 indicating a weight percentage of Te:
60.6%, Sb: 28.8%, and Ge: 10.6%.....30
14. Aggregation and coalescence of nanoparticles on the 12-hour ball milled sample
as a result of the ball milling process developing larger mean particles..... 34

1. Introduction to Thermoelectric Materials

1.1 Principles of Thermoelectrics

Thermoelectric (TE) materials can convert heat into electricity directly or vice versa. This phenomenon was first observed by Thomas Johann Seebeck in 1821 [1]. TE materials function through several different mechanisms. The Seebeck effect is a phenomenon that produces a voltage when there exists a temperature gradient between two dissimilar metals [1]. A diagram of how this phenomenon can be integrated into commercial applications can be seen in Fig. 1 below.

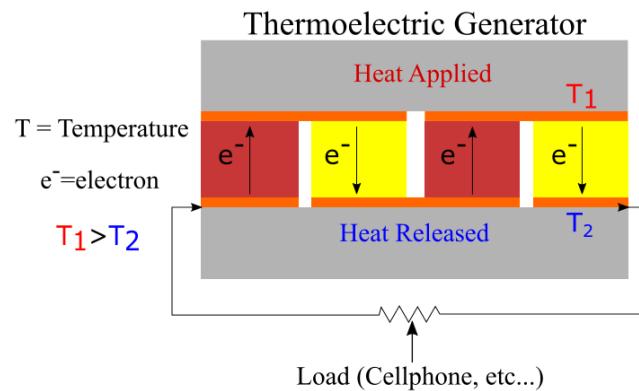


Fig. 1: Diagram of thermoelectric generator and working mechanisms.

In addition to the Seebeck effect, TE materials can work by means of the Peltier effect and Thomson effect. The Peltier effect was first observed in 1834 by Jean Charles Athanase Peltier who observed how an electric current would produce a temperature gradient in a metal [1]. Years later in 1854, Lord Kelvin noticed a correlation between the Peltier and Seebeck effect and was able to predict a third TE effect [1]. This effect would become known as the Thomson effect. The Thomson effect describes the process of how

heat is absorbed or produced when an electric current is directed into a material with an existing temperature gradient [1]. Examples of products that have utilized the TE effects are thermocouples, refrigeration cooling systems, and power generators. An example of a thermoelectric generator can be seen in Fig. 1, where heat transfers to electrons [2]. When the electrons become excited, they transfer the heat energy to the heat release which is then used to generate electricity [2]. Obviously, these effects can be a useful tool in harnessing and manipulating waste-energy for a variety of commercial applications. TE materials can also be used to repurpose solar energy and for engine heat loss recovery. However, for TE materials to be considered for widespread commercial application, the efficiency must be dramatically improved. It has been reported by the Lawrence Livermore Laboratory that nearly 70% of all energy was wasted in the form of heat in 2018 [3]. As a result of this issue, it is necessary to further develop efficient TE materials to convert the waste-energy into useful energy. The efficiency of TE materials is characterized by a dimensionless figure of merit (ZT) defined as:

$$ZT = \frac{\sigma S^2 T}{\kappa_e + \kappa_L}, \quad (1)$$

where σ is the electrical conductivity, S is the Seebeck coefficient, T is the absolute temperature, κ_e and κ_L are the electronic and lattice thermal conductivity, respectively [4]. In a number of published journals and experiments pertaining to TE materials, the performance is also quantified by the power factor defined as:

$$\text{Power Factor} = \sigma S^2. \quad (2)$$

In order to be commercially competitive, TE materials need to achieve a ZT higher than 3 [4]. The highest reported experimental ZT is ~ 2.6 at 923K, and much lower at room temperature which is not of large benefit for most commercial applications [5]. Ouyang et al. reported a ZT of 7.4 at 800K in a molecular dynamic (MD) simulation [6], however, simulation results must be carefully examined because they generally require complicated fabrication techniques to develop the specific structures in the simulated models. Developing TE materials with an increased ZT has proven to be a difficult feat because of the relationship between κ_e and σ found in the Wiedemann-Franz law (WF) defined as:

$$\kappa_e = LT\sigma, \quad (3)$$

where L is the Lorenz number. This relationship can transform (1) to:

$$ZT = \frac{S^2}{L + \frac{\kappa_L}{\sigma T}}. \quad (4)$$

As we can see from (3), κ_e and σ are directly correlated. Therefore, reducing the κ_e will lead only to a marginal improvement in ZT. It is apparent from (4) that reducing the ratio of κ_L and σ can lead to an increased efficiency of the TE material. However, S is directly proportional to σ which can negate the improvement to the Seebeck coefficient. Likewise, κ_L and σ are closely correlated and most methods of decreasing κ_L come with a sacrifice of reducing σ .

1.2 Lattice Thermal Transport

In order to obtain a material with a high TE performance, the material must have a low thermal conductivity to avoid unnecessary heat loss to minimize heat transfer from the hot contact to the cold contact. This concept can be seen in (1) where the thermal conductivity is in the denominator. Because of the direct correlation of κ_e and σ found in (3), decreasing the κ_L is a more direct approach to increasing the ZT. A variety of literature alludes to how good TE materials should behave as a phonon glass/electron crystal (PGEC). This behavior is described as an enhanced phonon scattering that combines the structure of crystal and disorderly structures that reduce κ_L and sustains a useful electron mobility [7]. The theory presents an innovative method of reducing the lattice thermal conductivity by filling voids in a crystal structure with heavy atoms that would effectively increase the increasing phonon scattering [4]. In insulators, thermal conductance of heat travels as a result of collective atom vibrations called phonons. Lattice thermal conductivity in crystals can be calculated using the Boltzmann transport equation (BTE) as:

$$\kappa_L = \sum_{\lambda} c_{\lambda} v_{\lambda}^2 \tau_{\lambda}, \quad (5)$$

where λ represents the phonon mode, c represents the specific heat of the phonon mode, v represents the phonon group velocity, and τ represents the phonon relaxation time [4]. The phonon group velocity can be reduced through use of strain or introduction of phononic crystals [4]. The phonon scattering rate is denoted as τ^{-1} and is a function of several scattering mechanisms including: Umklapp processes, normal processes, electrons,

magnons, grain boundaries, nanoprecipitates, dislocations, strain fields, point defects, and displacement layers and is described by Matthiessen's rule seen below [4].

$$\tau^{-1} = \tau_U^{-1} + \tau_N^{-1} + \tau_e^{-1} + \tau_m^{-1} + \tau_{GB}^{-1} + \tau_{NP}^{-1} + \tau_D^{-1} + \tau_S^{-1} + \tau_{PD}^{-1} + \tau_{DL}^{-1} + \dots \quad (6)$$

It would be useful to combine several of these scattering mechanisms resulting in a maximized reduction in lattice thermal conductivity. However, most nanotechnological methods of reducing the lattice thermal conductivity, also reduce the electrical conductivity which negates the purpose. Each of the influences of the scattering mechanisms mentioned in (6) effect the electrical and lattice thermal conductivity to different extents [4]. For instance, Qiu et al. demonstrated that Si can have a reduced thermal conductivity without deteriorating the electrical conductivity [8]. The thermal conductivity was reduced to approximately 30% for the phonon mean-free path of 100 nm [8]. This implies that with a critical dimension of 100 nm, the κ_L is reduced to nearly 30% of the bulk value. Meanwhile the electrical conductivity retained nearly the same electrical conductivity value of bulk Si. This example validates the notion that specific materials or grain sizes can affect κ_L and σ to different extents.

2. Thermoelectric Materials

Materials used for TE applications have their respective benefits and drawbacks. The materials have been studied in a range of dimensions from polycrystals to nanowires and films. Different materials will have different phonon scattering mechanisms. As seen

in Fig. 2 below, the choice of material will dictate which combination of phonon scattering processes will be used.

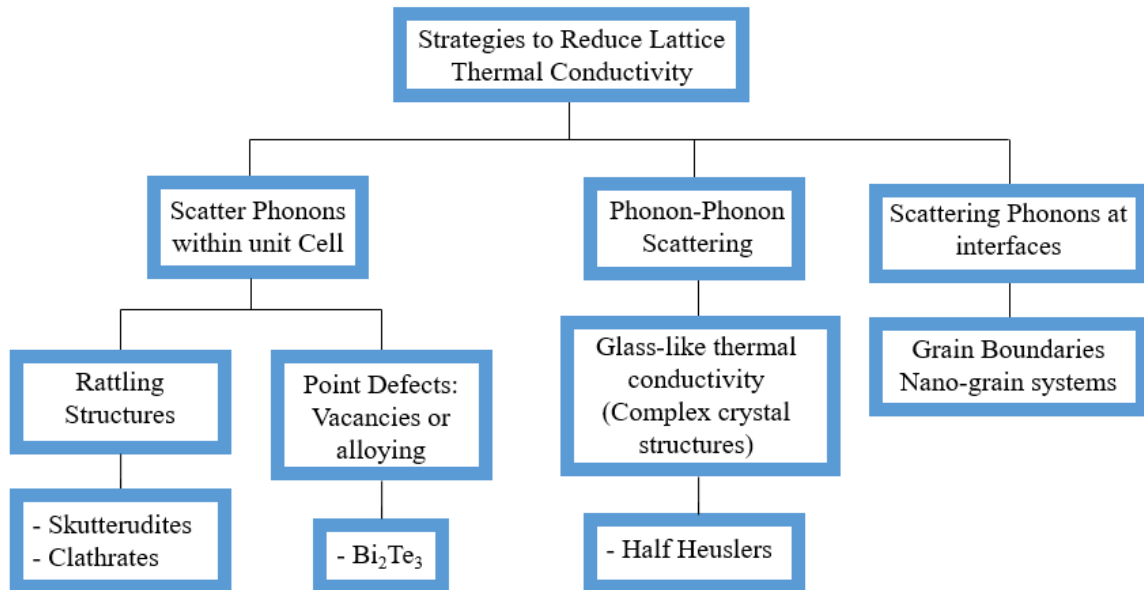


Fig. 2: Different phonon scattering mechanisms utilized by materials to reduce the lattice thermal conductivity.

The most popular TE materials in literature are semiconductors because the ratio of thermal to electrical conductivity is not fixed. Most of the advanced TE materials are defined by their nanostructuring [9]. These materials can be categorized by their distinct properties including fine grain sizes, dispersed particles, nano-inclusions and atomic defects [9]. These distinct characterizations make up an area of materials referred to as nanocomposites. Nanocomposites are effectively materials that have integrated a variety of nanoengineered particles into a single material. These materials have the ability to significantly improve the material properties in comparison to the bulk material. Nanostructuring these materials holds a promising future in the ability to independently

influence the S , σ , and κ_L . Nanostructuring demonstrates great potential in reducing the lattice thermal conductivity due to the increase in introduction of grain boundaries and nanoparticle interfaces that scatter phonons more effectively. This increased density of boundaries and interfaces allows for easy transport of electrons, while acting as strong phonon scattering mechanisms. There are a variety of nanocomposite materials under consideration for TE application including half-Heuslers, skutterudites, Bi_2Te_3 , and phase change materials such as $\text{Ge}_2\text{Sb}_2\text{Te}_5$. The reason these materials are popular considerations for TE applications is because they demonstrate a low lattice thermal conductivity due to the strong lattice anharmonicity, minimal phonon group velocity, and the strong phonon scattering properties introduced by material defects [4].

2.1 Half-Heuslers

Half-Heusler alloys have become a popular material for TE application due to their high temperature stability and therefore good potential for high temperature TE power generation [9]. The half-Heusler alloys have the chemical formula ABX ($A = \text{Zr, Hf, La}$; $B = \text{Pt, Ni}$; $X = \text{Bi, Sn}$). In this formula, A and B elements can be substituted to drastically reduce the lattice thermal conductivity while X can be substituted to enhance the electrical conductivity [10]. Half-Heuslers typically have a grain boundary size of several micrometers which allows efficient lattice thermal conductivity [9]. Decreasing the grain size can significantly increase the amount of phonon scattering that occurs. Another factor that lead to a decreased thermal conductivity of the half-Heuslers is phonon scattering by large differences in atomic mass [10]. Theoretically, the difference in atomic mass creates

a large local stress between the atoms bond and therefore strengthens the phonon scattering. This difference in mass combined with grain boundary size does not significantly increase the ZT, however, it allows the peak ZT to be reached at lower temperatures which allows for a more realistic application consideration. Half-Heuslers have only been able to achieve ZT of ~ 0.5 until recently due to their high thermal conductivity [10]. Huang et al. have made the breakthrough of increasing the ZT from 0.5 to 0.8 in p-type half-Heuslers and from 0.8 to 1 in n-type [10]. This increase in ZT can be attributed to their use of high energy ball milling to attain desired grain size and the hot-pressing procedure. They found that the average grain size from the fabrication process was about 100-300 nm which in turn, increases the grain surface density and enhances phonon scattering [10]. Additionally, they found that using elements with a larger size and mass difference enhanced the alloy scattering which allowed the peak ZT to be reached at a lower temperature which makes it more practical for commercial applications. Overall, the tunability of half-Heusler materials to reach higher ZT levels shows a promising future.

2.2 Skutterudites

Skutterudites typically have the formula MX_3 ($M=Co, Rh, Ir$; $X=P, As, Sb$) and utilize the PGEC mechanism to scatter phonons [4]. As shown below in Fig. 2, the voids of the crystal structures are occupied by heavier atoms that develop weak bonds with the host atoms and produces vibrational modes that greatly reduce lattice phonon transport [11]. While the filler atoms are predicted to reduce the lattice phonon transport by introducing strong anharmonicity, the filler atoms have also demonstrated an increased

electrical conductivity [11]. The fillers are typically elements with an electropositive charge, and therefore have a minimal effect on the band structure which allows the Seebeck coefficient to remain the same [11].

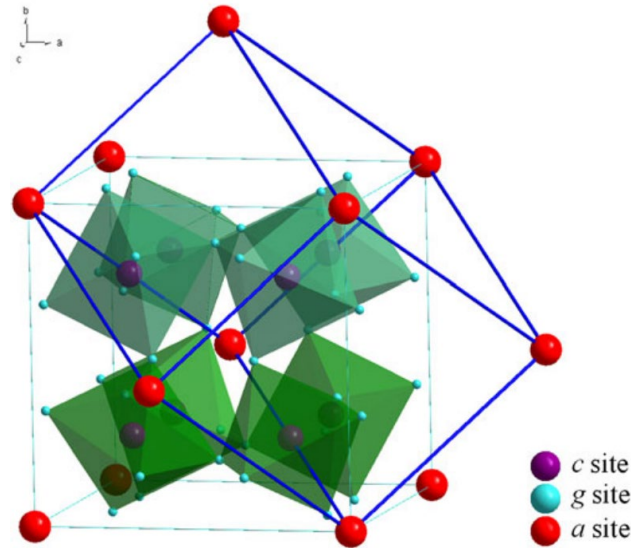


Fig. 3: Unit cell of CoSb_3 skutterudite. Co occupies 'c' sites, Sb occupies 'g' sites, and filler atoms may occupy the 'a' site. Reproduced with permission from [12].

Additionally, there has also been a correlation drawn between the number of filler atoms from different groups and the reduced thermal conductivity of the cell. Modeling the atoms as a spring and mass system allows for the calculation of the natural frequencies based on the ratio of the stiffness constant and mass. Atoms from different groups have much different natural frequencies and therefore can have a remarkable combined phonon scattering effect [9]. Another effective method of reducing the thermal conductivity in skutterudites has been through nanostructuring. Nanostructuring refers to the fabrication of the materials through manipulation of the powders and methods of compacting while

keeping the nanosized structure intact [11]. This method of reducing the lattice thermal conductivity is still a new and recent development which requires more experimental corroboration. The nanostructuring aims to reduce the grain sizes to around 200 nm which can greatly reduce the thermal conductivity [11]. This can be achieved through high energy ball milling and hot pressing. The hot-pressing compaction technique has been shown to have a pronounced impact on the TE properties of the materials. Yan et al. found that samples that underwent hot pressing over a range of different temperatures did not exhibit any significant modifications in phase composition, lattice parameters, or structural properties [13]. However, they did find that the samples pressed at lower temperatures demonstrated higher porosities, lower relative densities, reduced grain size, which in turn, increased the electrical resistivity and decreased the lattice thermal conductivity [13]. Overall, these materials show a promising future based on the filler atoms introducing strong lattice anharmonicity and achieving low thermal conductivity through nanostructuring. However, skutterudites will need to achieve higher figures of merit at intermediate temperature to become more feasible for commercial applications.

2.3 Bi₂Te₃

Bi₂Te₃ materials have been a popular nanocomposite used for commercial TE materials because of their reasonably high ZT at room temperature [9]. These nanocomposites have been reported to maintain a figure of merit near 1 until recently a value of 1.3-1.8 was reported [9]. Similar to the methods of reducing thermal conductivity discussed above, Bi₂Te₃ nanocomposites can also be nanostructured to modify the

quantities and sizes of the grain boundaries and nano-inclusions. Misra et al. studied the effects of incorporating semi-metallic Bi in Bi_2Te_3 matrix and the effects on lattice thermal conductivity [14]. They fabricated the pellets by ball milling the powders and hot pressing the samples [14]. They found that the Bi nano-inclusions presented additional phonon scattering locations aiding in a significant reduction in thermal conductivity of the lattice [14]. Additionally, the nano-inclusions caused line defects in the material which further reduced the lattice conductivity. Overall, they found that the contribution of the wide size distribution of Bi particle sizes helped scatter a wider range of mean free paths of phonons [14]. The combined effect of nanoparticles and nanograins significantly aided in an increased ZT because of the associated increase in electrical conductivity as well as a decrease in thermal conductivity [14]. The use of Bi_2Te_3 as a TE material shows a lot of promise for increasing the ZT in the room temperature range to a commercially competitive value.

2.4 $\text{Ge}_2\text{Sb}_2\text{Te}_5$

$\text{Ge}_2\text{Sb}_2\text{Te}_5$ (GST) compounds have just recently become materials of interest for TE applications. These materials are popular in the optical recording and phase-change random access memories systems (PCRAMS) because they can rapidly transform phases from an amorphous state to crystalline when exposed to heating above the glass transition temperature. The transition can form two different crystalline structures. The structures both contain a high density of vacancies which causes the cell to have a low thermal conductivity and high electrical conductivity [15]. For this reason, GST should

demonstrate excellent TE properties because of the heavy elements, large unit-cell measurements, and many vacancies [15]. As seen below in Fig. 3, the structure and thermal transport properties of the material are highly dependent on the phase of the material.

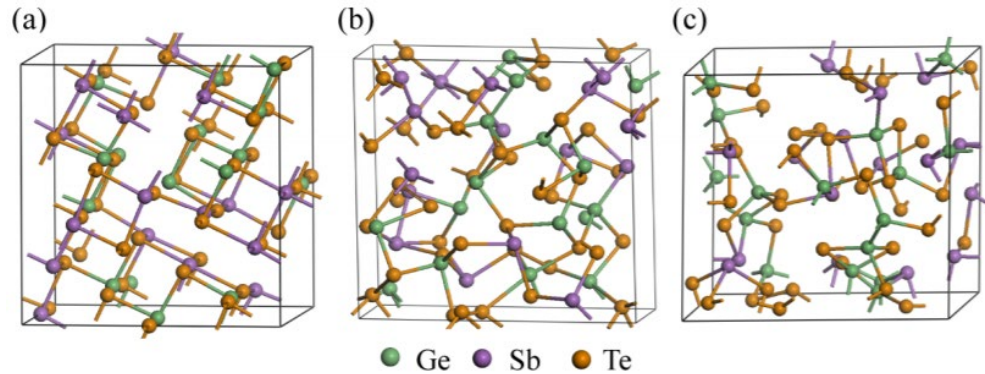


Fig. 4: Unit cell structure of the a) crystalline phase, b) melt quenched glass, c) ideal glass of $\text{Ge}_2\text{Sb}_2\text{Te}_5$. Reproduced with permission from [16].

Lan et al. studied the temperature dependence of the electrical and thermal conductivity of GST [17]. While most investigations of the properties of GST are focused on the thin films that are used in optical recording and PCRAMS, Lan et al. chose to investigate the thermal and electrical properties of the bulk material to analyze GST's potential for TE applications. They found that at room temperature, the thermal conductivity due to electron transport contributed nearly 80% of the bulk thermal conductivity [17]. They attributed the high electron thermal conductivity to the crystal structure of GST [17]. The typical quasi-stable GST crystal has Te atoms occupying one lattice site while Ge and Sb are randomly distributed amongst the second lattice site [17]. This random distribution produces a high vacancy density which allows for a high electrical conductivity and due to the WF law, a high thermal conductivity due to electron transport

[17]. In addition to the findings by Lan et al., Sankar et al. investigated how the manufacturing process may enhance the disorder in the crystal structures, and therefore increase the phonon scattering [18]. Sankar et al. found that by modifying the amount of germanium content in the substance without any impact on the crystal structure, they introduced more vacancies [18]. These vacancies improved the electrical conductivity and figure of merit from 0.7 to 1.1 at room temperature [18]. Additionally, by cooling the sample immediately after annealing, the ZT was increased from 1.1 to 1.48 due to the increase in disorder in the crystal structure which scattered more phonons [18]. With the recent findings of the excellent TE properties of GST, it is necessary to continue developing methods of increasing the ZT of the material.

2.5 Nanoparticle Size Distribution

While it has been demonstrated that the nanograins and nanoparticles can significantly contribute to a reduced lattice thermal conductivity, most literature on nanocomposites assume the nanoparticles to be of uniform size. More recent research has begun to focus on how a particular nanoparticle size distribution may affect the thermal conductivity of a nanocomposite. Zhang et al. demonstrated how it is unlikely for a single nanoparticle size to scatter phonons with a wide range of mean free paths [19]. However, they suggest that the best method of scattering a wide range of phonon mean free paths is not by having a broad distribution of nanoparticle radii but instead by introducing several discrete peaks of particular radii [19]. Zhang et al. found through MD simulations of SiGe that the optimal size distribution of nanoparticles to reach a minimum thermal conductivity

is a discrete size distribution [19]. Furthermore, they found that even when using the same size nanoparticle radii, the thermal conductivity was reduced to a value below amorphous Si [19]. These results are critical because they present a greatly reduced thermal conductivity that does not require an extreme manufacturing process. Huang et al. conducted a similar investigation on the effect of the mean and standard deviation of the nanoparticles radii on the overall thermal conductivity of the nanocomposite [20]. They found the larger the mean radius of the nanoparticles, the larger the thermal conductivity. This correlation can be explained by Eq. (7) below:

$$\Phi = \frac{3\varphi}{r}, \quad (7)$$

where Φ represents the interface density, φ represents the volume fraction of nanoparticles in the cell, and r represents the mean radius [20]. The smaller the interface density, the less blocking of thermal conductance through filler atoms occurs. Additionally, they found that the higher the standard deviation of nanoparticle radii, the higher the thermal conductivity of the nanocomposite [20]. When the standard deviation of the nanoparticles radii is relatively low ($\sigma < 13$), the thermal conductivity of the nanocomposite is much closer to a nanoporous material [20]. These investigations yielded helpful insights into the potential of nanocomposites further increasing their figures of merit through nanoinclusions. However, there are not many experiments to corroborate these numerical findings.

With the results regarding the nanoparticle size distribution, it is apparent that thermal conductivity is correlated to both the nanoparticle radii distribution and the

interface density in the nanocomposite. As depicted in Fig. 3, the methods of implementing a radii distribution and an increased interface density can be done in several ways.

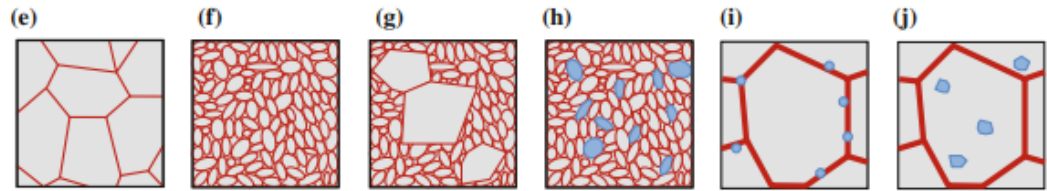


Fig. 5: General methods of improving phonon scattering through structure modification [21]. Represented above are e) micrometer grains, f) nanometer grains, g) mixture of different sized grains, h) mixture of nanoparticles with a variety of compositions, i) compaction of a mixture of two components, j) nanosize precipitates within bulk material. Adapted by permission from [Nature] [Journal of Materials Science] [Composite thermoelectric materials with embedded nanoparticles, Yi Ma, Richard Heijl, Anders E. C. Palmqvist] [2012] [21].

The developments and findings of nanocomposite related research and techniques of decreasing the lattice thermal conductivity for TE applications have been reviewed with an emphasis on the consideration of the materials, fabrication processes, and underlying mechanisms of thermal transport in nanocomposites. To further the implementation of TE materials in the renewable energy industry, the understanding of how materials can have their properties manipulated at a nanoscale level to enhance the properties to optimize the figure of merit is critical. From the several experiments and simulations that have been discussed, a basic understanding of the thermal transport mechanisms, simulation and modeling techniques for molecular dynamic investigations, material selection criteria, and processing parameters influence on the results, have been described.

3. Experimental and Simulation Investigation

3.1 Background and Motivation

In this study, $\text{Ge}_2\text{Sb}_2\text{Te}_5$ samples will be fabricated due to its unique and ultrafast phase-change properties that allow for the fine tunability of the TE properties based on the phase of the material. The phase change properties have been widely studied, however, the TE properties have yet to be investigated in depth. The studies that have investigated the TE properties have focused on thin-films rather than bulk materials that would be more applicable to commercial use. It is hypothesized that fabricating a nanocomposite with a discrete nanoparticle size distribution can reduce the thermal conductivity to optimize the material for TE applications. It is predicted that through the use of a variety of high energy ball milling durations, a desirable particle size distribution can be achieved to attain a decreased thermal conductivity as a result of an increase in grain boundary and nanoparticle interface densities. In this study, we fabricate several nanocomposites that have been ball milled for a variety of time durations and cold sintered at a constant temperature and pressure to interpret the correlation in number of grain boundaries and thermal conductivity of the samples. The samples thermal conductivity values were evaluated using a Laser Flash Apparatus. We also set out to confirm our findings with molecular dynamic simulations demonstrating a decrease in grain size of a polycrystal leads to a decrease in thermal conductivity of a nanocomposite.

3.2 Molecular Dynamic Simulation of Thermal Transport in Polycrystals

In a study to theoretically verify the hypothesis that an increased grain boundary density will increase the number of phonon scattering mechanisms, and in turn, decrease the thermal conductivity of the material, a simulation was conducted using the LAMMPS package [22]. The simulation was conducted on solid argon at a temperature of 30 K. The interactions between the atoms was calculated within the framework of the Lennard-Jones potential. The simulations were set to compare the thermal conductivity of a single crystal, 4 grains, 8 grains, 16 grains, and 32 grains in a 10 nm by 10 nm by 10 nm cube containing around 27,000 atoms. In order to calculate the initial values, the atoms were arranged using coordinate files developed in MATLAB and AtomsK which modeled a face-centered cubic lattice for solid argon [23]. In most cases, estimating the thermal conductivity of real materials can be costly and inaccurate because the calculation requires a semiempirical characterization of the interatomic interactions. However, in the case of argon, it has been found that the interatomic interactions can be described with reasonable accuracy by the simple Lennard-Jones (LJ) potential:

$$\varphi(r_{ij}) = 4\varepsilon \left[\left(\frac{\sigma}{r_{ij}} \right)^{12} - \left(\frac{\sigma}{r_{ij}} \right)^6 \right], \quad (8)$$

where r_{ij} represents the distance between the atoms i and j [24]. In order to clearly demonstrate the phonon scattering effects the grain boundaries have on the thermal conductivity of a material in the simulation, the parameters $\varepsilon = 16\varepsilon_{AR}$ eV and $\sigma_{AR} = 0.34$ nm were used. In this study, $\varepsilon = 0.1664$ eV is used for the zero-potential-energy pair

between atoms i and j to emulate the interactions of materials with much stronger bonding than argon such as $\text{Ge}_2\text{Sb}_2\text{Te}_5$ to more accurately compare with our experimental findings. The macroscopic lattice thermal conductivity of the solid argon is calculated using the Green-Kubo formalism. This approach calculates the thermal conductivity using the following formula:

$$\kappa = \frac{V}{k_B T^2} \int_0^\infty \langle J_x(0) \cdot J_x(t) \rangle dt = \frac{V}{3k_B T^2} \int_0^\infty \langle J(0) \cdot J(t) \rangle dt, \quad (9)$$

where V is volume, T is the temperature, and J is the microscopic heat current, and the brackets $\langle \rangle$ denote autocorrelation [24]. The microscopic heat current is calculated by:

$$j(t) = \sum_j v_j \epsilon_j + \frac{1}{2} \sum_{i,j,i \neq j} r_{ij} (F_{ij} \cdot v_i), \quad (10)$$

where v_i is the velocity of particle i , and F_{ij} is the force on particle i from the paired particle j .

MD simulations were conducted in both the NPT (constant pressure and temperature) and NVE (constant volume and energy) ensembles to allow for comparison with published literature. The periodic boundary condition is applied to all three directions. The simulation conducted an initial NPT command to elevate the temperature from 0 to 30 K to ensure a stable structure in a solid state. Then, an additional NPT command was conducted to relax the structure and reach the target temperature with zero pressure. A Nosé–Hoover thermostat is introduced to maintain a constant temperature. The structure is then subjected to the NVE ensemble in which the instantaneous heat flux is recorded. Then

the Green-Kubo formalism (Eq. 9) is used to calculate the thermal conductivity of the structures. The integration time step was 1 fs with a cutoff radius of 5 angstrom and a periodic boundary condition to ensure an accurate assessment of all pairing interactions were considered. The simulated structures containing 4, 8, 16, and 32 grains can be seen below in Fig. 5.

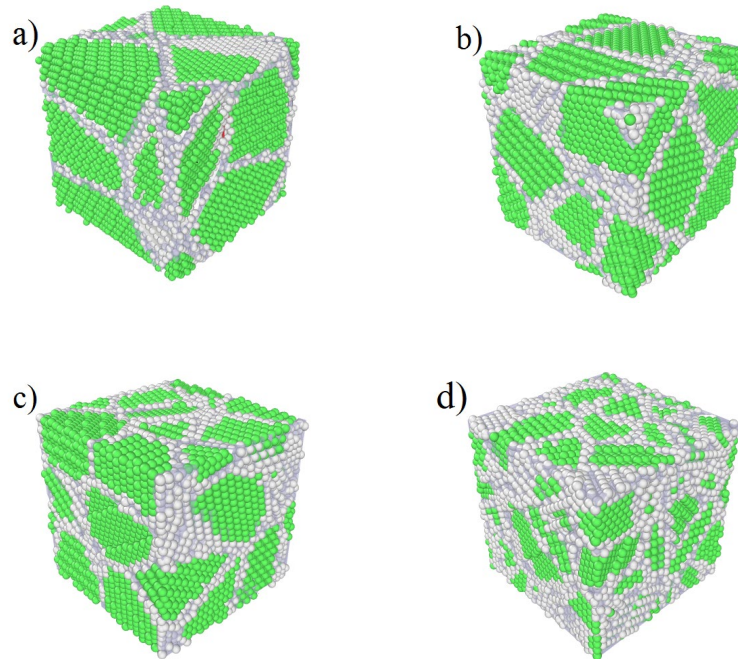


Fig. 6: The simulated structures generated by AtomsK containing a) 4 grains b) 8 grains c) 16 grains and d) 32 grains [23]. The green, white, and red spheres represent FCC, amorphous, and HCP structure types, respectively. Note that the structure in panels a-d seem to have more than the designated number of grains, which is merely a result of the periodic boundary condition used in OVITO.

3.3 Experimental Investigation of Thermal Transport in Polycrystalline $\text{Ge}_2\text{Sb}_2\text{Te}_5$

3.3.1 $\text{Ge}_2\text{Sb}_2\text{Te}_5$ Sample Preparation

$\text{Ge}_2\text{Sb}_2\text{Te}_5$ ingots (99.9% purity) were purchased from Process Materials Inc. The ingots were ground into powder form by hand using a ceramic mortar and pestle. The powders were ground until the particles had a diameter less than ~ 1 mm and ready to be placed into the ball mill. The ball milling process is a high energy impact method used to grind or blend materials. The powder is loaded into a cylindrical shell containing grinding media such as steel or zirconia spheres of different sizes. The ball mill rotates the cylinder about its axis and the grinding media impacts the powder which reduces the size of the particles. The ball mill used to grind the materials was an MTI High Speed Ball Mill (MSK-SFM-3). This model offers a higher impact energy than typical ball mills which is a result of the rotation, vibration, and oscillatory motion that is provided to the cylindrical shell. The powders were placed into the ball mill for a variety of time durations to analyze the effect of particle size on thermal conductivity.

After the ball milling procedure, the powder was then pressed using an MTI 15T Hydraulic Press with 0.5" Heatable Die Cold Sintering Press (YLJ-CSP-15). The cold sintering press fabricates pellets from the GST powder as seen below in Fig. 7.



Fig. 7: Images of GST powder before grinding and ball milling process (left) and fabricated pellet (GST-4) as a result of the cold sintering press (right).

The cold sintering process is a recent, innovative method to achieve dense solids at much lower temperatures than previously needed for sintering. This method of sintering is very popular in the fabrication of ceramic or ceramic-polymer composites, semiconductors, and materials with desirable dielectric properties because of its extremely low operating temperatures. The lower pressing temperature has also been shown to prevent the coarsening of the nanopowders, demonstrate higher electrical resistivity, and lower the thermal conductivity as demonstrated in Ref. 13. The cold sintering process uses aqueous-based solutions to increase the density through a dissolution-precipitation process [25]. The press can provide a temperature of up to 250°C and 1200 MPa. The parameters of the fabrication process for the samples were kept uniform to ensure the differences in thermal conductivity measurement were a result of particle size from the ball milling process. The parameters used to fabricate each 12.75 mm diameter sample can be seen below in Table 1. The variation in sample mass and thickness is a result of the ball milling process.

Table 1: Ge₂Sb₂Te₅ sample fabrication parameters.

Sample Name	Pellet Mass [g]	Thickness [mm]	Density [g/cm³]	Ball Mill [RPM]	Ball Mill Time [Hrs]	Press Time [min]	Press Temperature [C]	Press Pressure [MPa]
GST-1	1.3	1.87	5.4	540	1	10	170	600
GST-2	1.63	2.3	5.6	540	2	10	170	600
GST-3	1.33	1.91	5.5	540	3	10	170	600

3.3.2 Experimental Procedure

After the samples had been pressed into pellets, the thermal conductivity was evaluated using a NETZSCH LFA 447 Nanoflash. The laser flash method is common in measuring the thermal properties of materials due to its short measurement time, ability to evaluate a range of thermophysical properties, and ability to manipulate the output graphs of thermal diffusivity, thermal conductivity, or specific heat. This method of evaluation consists of a plane-parallel sample that is heated with a short burst from a xenon flash lamp. As seen in Fig. 8, the flash lamp is contained in a parabolic reflecting container to ensure a homogeneous illumination of the face of the sample.

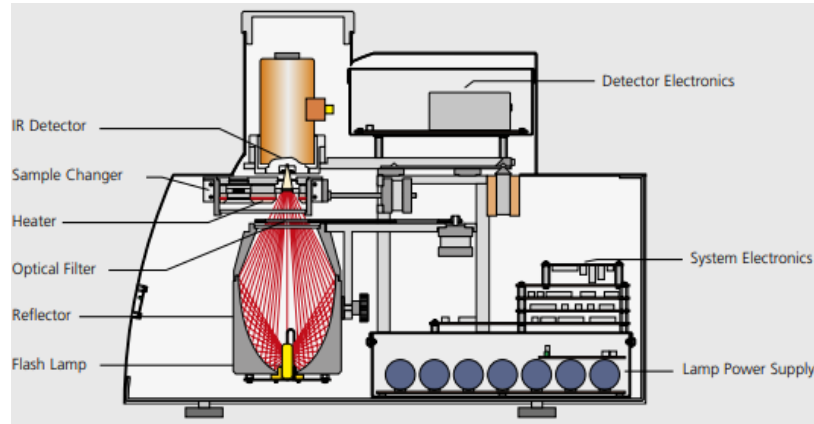


Fig. 8: Schematic of components of LFA 447 [26].

The resulting time dependent temperature rise on the rear surface is measured using an infrared (IR) detector. From this measurement, the thermal diffusivity and specific heat can be calculated simultaneously, and in turn, the bulk thermal conductivity can be calculated if density is known. The thermal diffusivity of the sample is evaluated using Eq. (11) seen below:

$$a = 0.1388 \cdot \frac{d^2}{t_{1/2}}, \quad (11)$$

where a is thermal diffusivity, d is the thickness of the sample, and $t_{1/2}$ is the time to half the maximum temperature rise [26]. The relationship to determine the thermal conductivity is demonstrated in Eq. (12) below:

$$\lambda(T) = a(T) \cdot c_p(T) \cdot \rho(T), \quad (12)$$

where $\lambda(T)$ is the bulk thermal conductivity as a function of temperature, $a(T)$ is the thermal diffusivity as a function of temperature, $c_p(T)$ is the specific heat as a function of

temperature, and $\rho(T)$ is density as a function of temperature [26]. NETZSCH recommends adding a layer of graphite lubricant to both sides of the samples to enhance the absorption and transmission of the laser energy to the IR detector. This graphite coating not only improves the signal-to-noise ratio of the measurement, but also ensures the surface of the sample is uniform and reduces reflectivity of the laser pulse.

4. Results and Discussion

4.1 Results of Molecular Dynamic Simulations

As seen below in Table 2, the increasing number of grains in the unit cell results in a severe reduction of thermal conductivity. Table 2 portrays the average thermal conductivity taken from the first 10,000-time steps and clearly indicates a trend of reduction of thermal conductivity with a decreasing grain size. The average grain length is derived Eq. (13) below:

$$\text{Average Grain Length} = \sqrt[3]{\frac{V}{N}} \quad (13)$$

where V is the volume of the cubic structure and N is the number of grains in the structure.

Table 2: Comparison of the simulation results for thermal conductivity of solid argon with varying number of grains per structure.

κ Dependence on Grain Length			
# of Grains	Average Grain Length [nm]	# of Time Steps [fs]	κ_{avg} [W/mK]
Single	0	10000	73.4
4	6.366	10000	1.9
8	5.066	10000	1.7
16	4.029	10000	1.6
32	3.199	10000	1.5

As seen in Fig. 9 below, the dependence of the thermal conductivity of solid argon on the number of grains in the cell is clearly demonstrated. Because the thermal conductivity of the single crystal data is so high, it has been omitted from the plot to provide a clear depiction of the influence an increasing number of grains has on the thermal conductivity. This graph representation clearly indicates the introduction of the increasing number of grains reduces the phonon mean free path and therefore increases the number of phonon scattering mechanisms. These results can be attributed to the introduction of an increasing number of grain boundaries and nanoparticle interfaces.

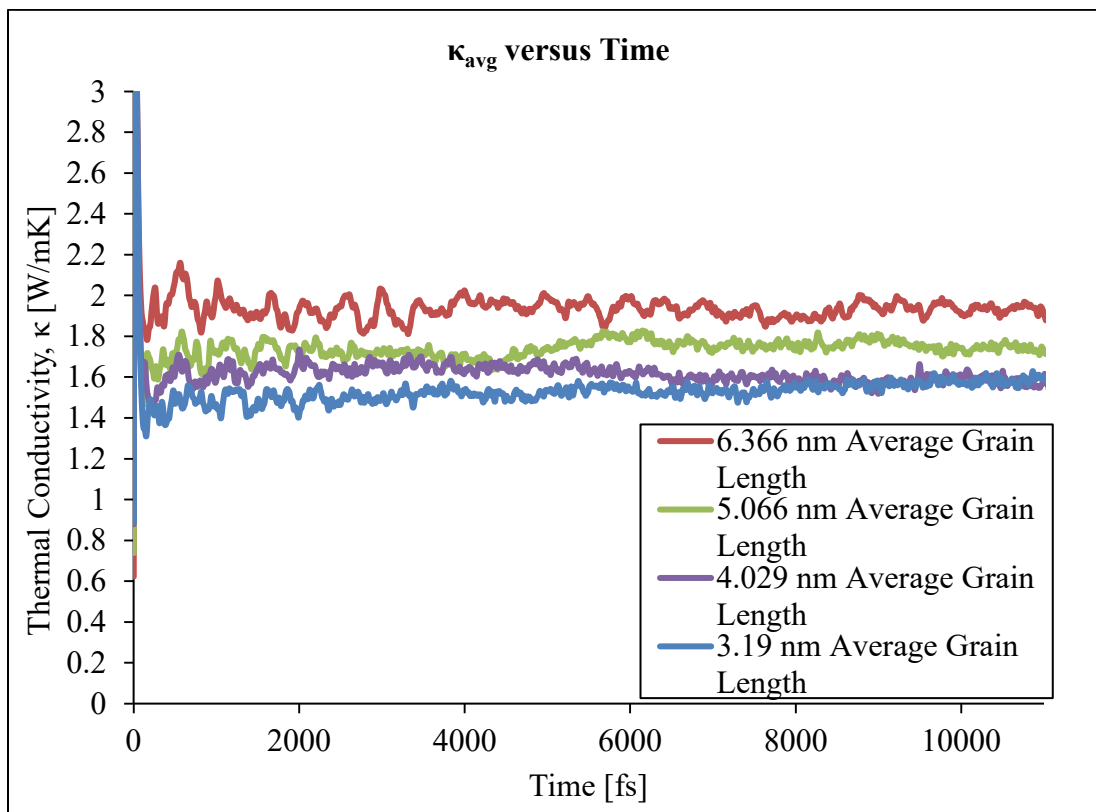


Fig. 9: Grain size dependence of the thermal conductivity of solid argon at 30 K over 10000 time steps. The average thermal conductivity of single-crystalline sample is 73.4 W/mK, as predicted by our molecular dynamic simulations.

This finding of the decreased thermal conductivity is in agreement with published literature on MD simulations investigating the effects of increasing number of phonon scattering mechanisms such as grain boundaries and nanoparticle interfaces.

4.2 Results of Thermal Conductivity Measurements

The results of the thermal conductivity measurements from the LFA analysis for the $\text{Ge}_2\text{Sb}_2\text{Te}_5$ samples can be seen below in Fig. 10.

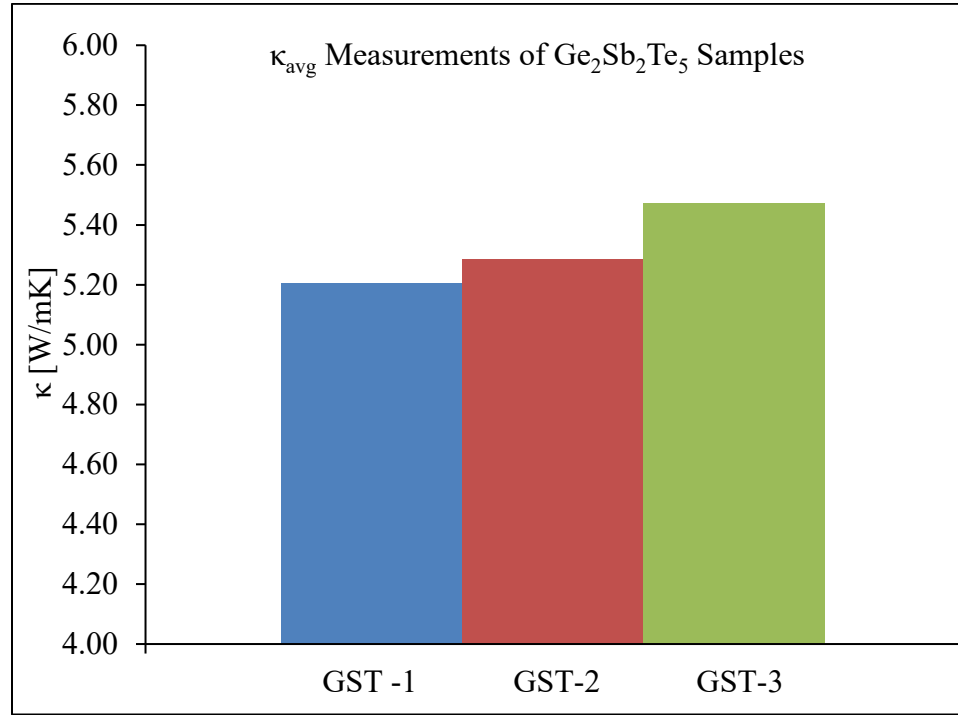


Fig. 10: Average bulk thermal conductivity measurements of GST samples.

The results of the LFA analysis are much higher than anticipated for the GST samples. The standard deviations and average thermal conductivity values of the measurements for each sample can be found in Table 3.

Table 3: Average thermal conductivity and standard deviations of the GST samples as measured by the LFA.

Sample Name	Pellet Mass [g]	Thickness [mm]	Ball Mill Time [Hrs]	κ_{avg} [W/mK]	σ [W/mK]
GST-1	1.3	1.87	1	5.20	0.0531
GST-2	1.63	2.30	2	5.28	0.0325
GST-3	1.33	1.91	3	5.47	0.0179

4.2.1 SEM Analysis

To verify the composition and surface structure of the $\text{Ge}_2\text{Sb}_2\text{Te}_3$ samples, a sample that was ball milled for 12 hours was analyzed using scanning electron microscopy (SEM) and energy dispersive x-ray spectroscopy (EDS). The equipment used for the surface micrographs was a JEOL JSM-7100FT Field Emission Scanning Electron Microscope (FESEM). FESEM is a process utilizing a high-energy beam of electrons to produce an image. When the electrons come into contact with the sample, they can produce a scattering of electrons, secondary electrons, or X-rays [27]. These signals are collected by the equipment sensors and are used to form an image on the screen. The FESEM surface micrographs of two different locations on a sample that was ball milled for 12 hours can be seen below in Fig. 11.

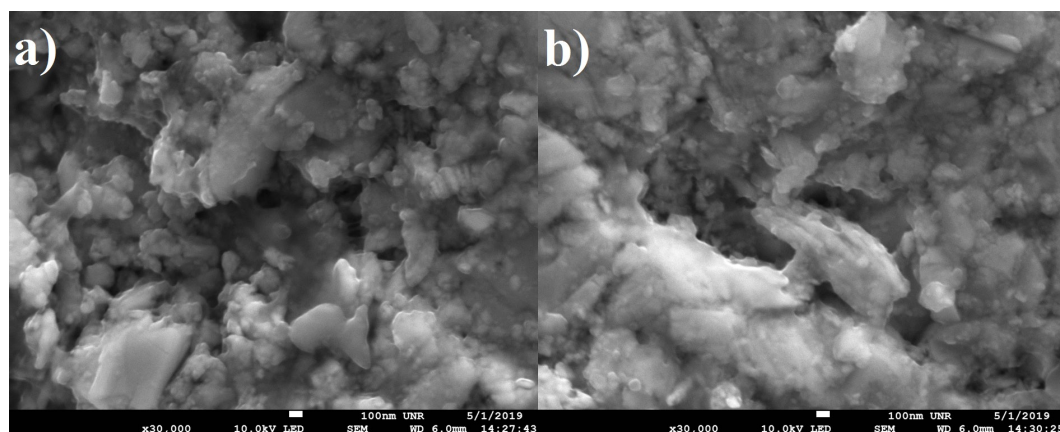


Fig. 11: SEM surface micrographs of a) location 1 and b) location 2 on a 12-hour milled sample.

Prior to FESEM analysis, the sample was prepared using an EcoMet 300 Grinder Polisher with SiC polishing material. The sample was polished for one minute at a rotating speed of 30 rpm. The polishing intended to rid of any remaining graphite lubricant on the sample surface from the LFA analysis. The FESEM micrographs were taken at a high vacuum of 8.6×10^{-6} Pa and with an accelerating voltage of 10 kV at 30,000 times magnification. These settings were selected based on the high level of detail shown in the micrographs. From the FESEM micrographs, it can be determined that the cold sintering press increased the density of the samples and was successful in compacting many of the nanoparticles to develop larger nanoparticles. The smaller particles in the image are a result of the ball milling process and are estimated to be in the range of 200-300 nm in length. The larger particles are a result of the aggregation of individual particles. These finding indicates the simultaneous occurrence of breakage and aggregation during the ball milling process. The sample was then analyzed for molecular composition using EDS.

EDS analysis is a process that can determine the composition of the sample alongside the FESEM analysis. When the electron beam comes into contact with the surface, the electron vacancies are filled with electrons with a higher energy level. In turn, x-rays are emitted to balance the difference in energies [28]. The elements are characterized by the energy of the emitted x-rays [28]. The EDS software then evaluates the relative percentage of emitted x-rays in comparison to their respective energy levels and can determine the weight percentage or elemental composition of the sample [28]. The sample that was ball milled for 12 hours was analyzed for composition using EDS analysis.

The micrograph in Fig. 12 was examined and was found to have the weight percentage indicated in Fig. 13.

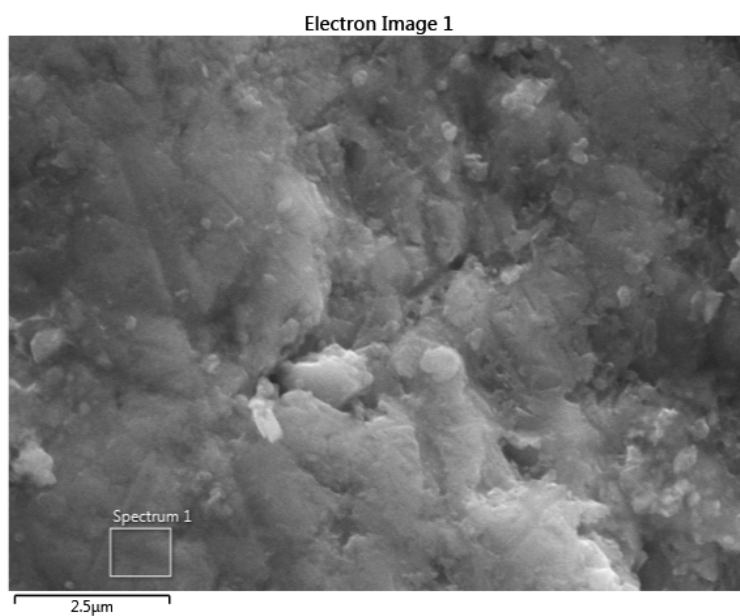


Fig. 12: Location used for EDS analysis containing area indicated in Fig. 11b.

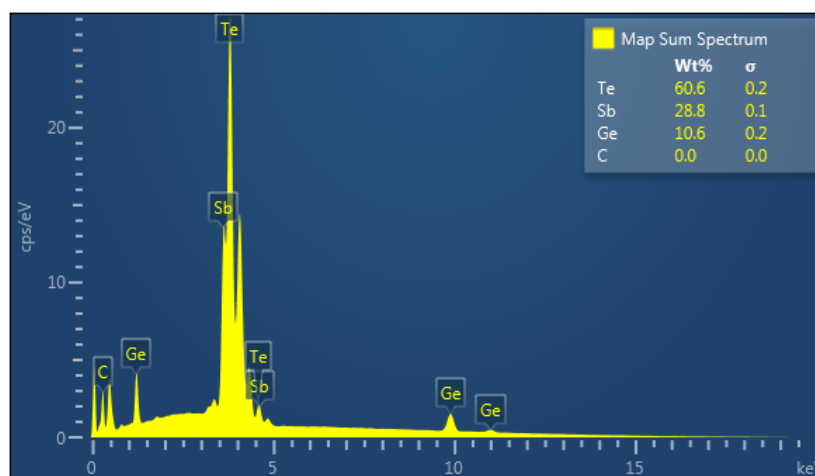


Fig. 13: EDS analysis of micrograph in Fig. 12 indicating a weight percentage of Te: 60.6%, Sb: 28.8%, and Ge: 10.6%.

The EDS analysis at several locations on the surface of the sample demonstrated a negligible fluctuation without prevalent positional variations in composition. The EDS results suggest a molecular formula of $\text{Ge}_2\text{Sb}_{3.2}\text{Te}_{6.5}$ which is higher than the nominal molecular composition of $\text{Ge}_2\text{Sb}_2\text{Te}_5$.

4.3 Discussion of Results and Experimental Errors

4.3.1 Discussion

The results of the MD simulation demonstrate a decreasing thermal conductivity as the number of grain boundaries and nanoparticle interfaces increase. The simulation findings are in good agreement with the trends found in Ref. 19 and Ref. 29.

The results of the experimental thermal conductivity analysis yielded unanticipated values. The thermal conductivity measurements exhibited an average bulk thermal conductivity of 5.32 W/mK. This value is much different than the thermal conductivity found in Ref. 30 of <1.5 W/mK for bulk GST. Not only are the thermal conductivity values of the samples much higher than anticipated, the values for each respective sample follow the opposite trend. The sample that experienced the longest ball milling time exhibited the highest thermal conductivity. It is believed that this trend is a result of particle aggregation and coalescence. Similar to the trend seen in Ref. 31, the aggregation and coalescence of the nanoparticles is a representation of the simultaneous grinding and development of nanoparticles. The distribution of the nanoparticles and the aggregation/coalescence of the nanoparticles can be seen in Fig. 11. The particle aggregation/coalescence demonstrates

the opposite of the desired outcome of the ball milling process. These aggregated particles increase the mean particle size and will allow for more efficient thermal conductivity through the sample. This aggregation and coalescence can be prevented through the use of wet milling rather than dry milling. Wet milling will include organic additives such as alcohols to prevent the agglomeration of the nanoparticles to form larger particles. The continued analysis of the results and sources of error can be found in chapter 4.3.2.

4.3.2 Experimental Errors

There exist a few possible sources of uncertainty regarding the experimental investigation and they are discussed in this section.

One possible source of error stems from the sample fabrication process. The variations in the sample mass and thickness can have a direct influence on the calculation of the thermal conductivity of the samples. As seen in Eq. (11), the thermal diffusivity as calculated by the LFA is proportional to the square of the thickness of the sample. The LFA user manual suggests a sample thickness of 1-1.5 mm for materials with a low diffusivity ($< 1 \text{ mm}^2/\text{s}$) [26]. The evaluated samples had a range of thicknesses from ~ 1.8 - 2.3 mm which may have had an influence on the high thermal diffusivity measurements. With the variation in sample thickness and mass, the density was also found to deviate slightly from a constant value. This variation in density influences the calculation of thermal conductivity as seen in Eq. (12).

However, considering the low standard deviation seen in each LFA measurement, the thickness, mass, and density should not influence the measurement to this magnitude. Additionally, the EDS analysis of the sample composition indicates an excess amount of Sb and Te in the sample from the nominal composition. This excess material would introduce an increased number of free electrons to aid in thermal transport, and in turn, increase the thermal conductivity measurements. The contribution of the excess electrons can be evaluated using a four-point probe resistivity measurement. This resistivity would then allow for the calculation of the electron contribution to thermal conductivity using the WF law. The suggestion of a large contribution of electron thermal transport to the bulk thermal conductivity is in alignment with the findings of Ref. 17 where the thermal conductivity contribution due to electrons was nearly 80% of the bulk materials thermal conductivity. This value would only increase with the presence of excess Sb and Te in the samples. The excess material also suggests the possibility of phase separation within the samples. Phase separation could introduce Sb_2Te_3 and influence the thermal properties of the samples.

The thermal conductivity measurements demonstrated an increase in value as the ball mill time increased. This is believed to be a result of the nanoparticle aggregation and coalescence seen below in Fig. 14.

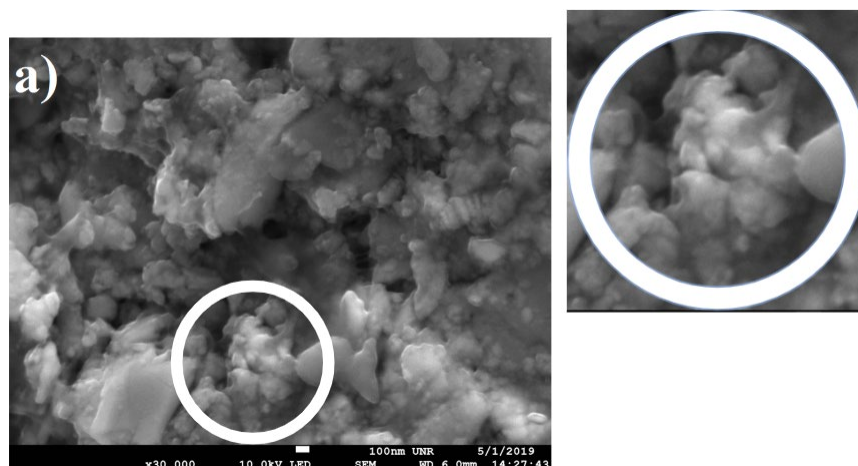


Fig. 14: Aggregation and coalescence of nanoparticles on the 12-hour ball milled sample as a result of the ball milling process developing larger mean particle sizes.

As the time duration of the ball milling process increases, the rate of particle breakage decreases. This is combination of the fact that smaller particles tend to be stronger and due to the tendency of particles to aggregate and form larger particles [32]. This agglomeration process can be abated through the use of the wet ball milling process which involves the addition of an organic solvent to lessen the particle aggregation/coalescence. This method of wet ball milling is claimed to decrease particle aggregation in Ref. 32.

5. Conclusion and Future Work

5.1 Conclusion

The purpose of this thesis experiment was to demonstrate through classical molecular dynamic simulation and experimental investigation how the nanostructuring of particle size in $\text{Ge}_2\text{Sb}_2\text{Te}_5$ nanocomposites can reduce the lattice thermal conductivity. The

average LFA evaluated bulk thermal conductivity of the samples was found to be 5.32 W/mK. While the thermal conductivity measurements are much higher than anticipated, the sources of error have been discussed in chapter 4.3.2.

The results of the MD simulation were found to be in good agreement with published literature. These findings indicate that the nanostructuring of the particle sizes in nanocomposites can have a significant influence on the lattice thermal conductivity of materials. While these simulation findings demonstrate the possible influence nanoparticles can have, simulations can only provide a certain level of insight to the fundamental mechanisms governing phonon transport in materials. The conditions in real life situations are not those of the ideal simulation parameters.

5.2 Future Work

There exists the potential for future work for the investigation of nanostructuring particle size in nanocomposites to reduce the thermal conductivity of materials. As demonstrated through the MD simulations, the increase in nanoparticle interface density leads to a significant reduction in lattice thermal conductivity. Future investigations should utilize the wet ball milling process when fabricating GST nanocomposites to prevent particle aggregation. The electron contribution to thermal conductivity should be calculated using the four-probe resistivity measurement method in combination with the WF law to calculate the estimated lattice thermal conductivity of the sample. The fabrication of TE nanocomposites should further investigate the best distribution of nanoparticle radii rather than utilizing uniformly sized nanoparticles. Determining an

optimized distribution of nanoparticle sizes within TE nanocomposites would increase the range of phonon wavelength scattering possibilities and further decrease the lattice thermal conductivity.

References

- [1] “Brief History of Thermoelectrics,” History of Thermoelectrics. [Online]. Available: <http://www.thermoelectrics.caltech.edu/thermoelectrics/history.html>.
- [2] A. scioto, “thermoelectric devices,” The Wonders of Innovative Science. [Online]. Available: <https://sites.suffolk.edu/scioto/2016/03/04/thermoelectric-devices/>.
- [3] “LLNL Flow Charts,” 2017, <https://flowcharts.llnl.gov/>.
- [4] P. Chakraborty, T. Ma, A. Zahiri, L. Cao, Y. Wang, “Carbon-Based Materials for Thermoelectrics,” *Advances in Condensed Matter Physics*, vol 2018.
- [5] L.-D. Zhao, S.-H. Lo, Y. Zhang et al., “Ultralow thermal conductivity and high thermoelectric figure of merit in SnSe crystals,” *Nature*, vol.508, no.7496, pp.373–377, 2014.
- [6] Y. Ouyang, Y. Xie, Z. Zhang, Q. Peng, and Y. Chen, “Very high thermoelectric figure of merit found in hybrid transition-metal-dichalcogenides,” *Journal of Applied Physics*, vol. 120, no. 23, p. 235109, 2016.
- [7] L. Wu, Q. Meng, C. Jooss, J.-C. Zheng, H. Inada, D. Su, Q. Li, and Y. Zhu, “Origin of Phonon Glass-Electron Crystal Behavior in Thermoelectric Layered Cobaltate,” *Advanced Functional Materials*, vol. 23, no. 46, pp. 5728–5736, 2013.
- [8] B. Qiu, Z. Tian, A. Vallabhaneni et al., “First-principles simulation of electron mean-free-path spectra and thermoelectric properties in silicon,” *EPL (Europhysics Letters)*, vol.109, no.5, p.57006, 2015 (English).
- [9] W. Liu, X. Yan, G. Chen, and Z. Ren, “Recent advances in thermoelectric nanocomposites,” *Nano Energy*, vol. 1, no. 1, pp. 42–56, 2012.
- [10] L. Huang, Q. Zhang, B. Yuan, X. Li, X. Yan, and Z. Ren, “Recent progress in half-Heusler thermoelectric materials,” *Materials Research Bulletin*, vol. 76, pp. 107–112, Apr. 2016.
- [11] M. Rull-Bravo, A. Moure, J. F. Fernández, and M. Martín-González, “Skutterudites as thermoelectric materials: revisited,” *RSC Advances*, vol. 5, no. 52, pp. 41653–41667, 2015.
- [12] X. Shi, S. Bai, L. Xi, J. Yang, W. Zhang, L. Chen, and J. Yang, “Realization of high thermoelectric performance in n-type partially filled skutterudites,” *Journal of Materials Research*, vol. 26, no. 15, pp. 1745–1754, 2011.

- [13] X. Yan, E. Bauer, P. Rogl, and S. Paschen, "Influence of hot pressing temperature on thermoelectric properties of type-I clathrates," *physica status solidi (a)*, vol. 211, no. 6, pp. 1282–1287, 2014.
- [14] D. Misra, S. Sumithra, N. Chauhan, W. Nolting, P. Poudeu, and K. L. Stokes, "Correlation between microstructure and drastically reduced lattice thermal conductivity in bismuth telluride/bismuth nanocomposites for high thermoelectric figure of merit," *Materials Science in Semiconductor Processing*, vol. 40, pp. 453–462, 2015.
- [15] A. V. Kolobov, P. Fons, A. I. Frenkel, A. L. Ankudinov, J. Tominaga, and T. Uruga, "Understanding the phase-change mechanism of rewritable optical media," *Nature Materials*, vol. 3, no. 10, pp. 703–708, 2004.
- [16] E. Cho, J. Im, C. Park, W. J. Son, D. H. Kim, H. Horii, J. Ihm, and S. Han, "Atomic and electronic structures of amorphous Ge₂Sb₂Te₅; melt-quenched versus ideal glasses," *Journal of Physics: Condensed Matter*, vol. 22, no. 20, p. 205-504, 2010.
- [17] R. Lan, R. Endo, M. Kuwahara, Y. Kobayashi, and M. Susa, "Electrical and Thermal Conductivity and Conduction Mechanism of Ge₂Sb₂Te₅ Alloy," *Journal of Electronic Materials*, vol. 47, no. 6, pp. 3184–3188, 2017.
- [18] R. Sankar, D. P. Wong, C.-S. Chi, W.-L. Chien, J.-S. Hwang, F.-C. Chou, L.-C. Chen, and K.-H. Chen, "Enhanced thermoelectric performance of GeTe-rich germanium antimony tellurides through the control of composition and structure," *CrystEngComm*, vol. 17, no. 18, pp. 3440–3445, 2015.
- [19] H. Zhang and A. J. Minnich, "The best nanoparticle size distribution for minimum thermal conductivity," *Scientific Reports*, vol. 5, no. 1, 2015.
- [20] C.-L. Huang, X. Qian, and R.-G. Yang, "Influence of nanoparticle size distribution on the thermal conductivity of particulate nanocomposites," *EPL (Europhysics Letters)*, vol. 117, no. 2, p. 24001, 2017.
- [21] Y. Ma, R. Heijl, and A. E. C. Palmqvist, "Composite thermoelectric materials with embedded nanoparticles," *Journal of Materials Science*, vol. 48, no. 7, pp. 2767–2778, 2012.
- [22] S. Plimpton, "Fast parallel algorithms for short-range molecular dynamics," *Journal of Computational Physics*, vol. 117, no. 1, 1993.
- [23] "Atomsk: A tool for manipulating and converting atomic data files" Pierre Hirel, *Comput. Phys. Comm.* **197** (2015) 212-219 | doi:10.1016/j.cpc.2015.07.012

- [24] P. Heino, “Thermal conductivity and temperature in solid argon by nonequilibrium molecular dynamics simulations,” *Physical Review B*, vol. 71, no. 14, 2005.
- [25] J. Guo, A. L. Baker, H. Guo, M. Lanagan, and C. A. Randall, “Cold sintering process: A new era for ceramic packaging and microwave device development,” *Journal of the American Ceramic Society*, vol. 100, no. 2, pp. 669–677, 2016.
- [26] Thermal Diffusivity - Thermal Conductivity, NETZSCH, Selb, Germany, pp. 4. Accessed on: April 29, 2019. [Online]. Available: <http://photos.labwrench.com/equipmentManuals/7515-2757.pdf>
- [27] “Scanning Electron Microscopy,” Nanoscience Instruments. [Online]. Available: <https://www.nanoscience.com/techniques/scanning-electron-microscopy/>. [Accessed: 02-May-2019].
- [28] “Energy Dispersive X-Ray Spectroscopy (EDS),” Energy Dispersive X-Ray Spectroscopy | EDS Failure Analysis | EDS Material Analysis | EDX Failure Analysis | EDX Material Analysis. [Online]. Available: <https://www.mee-inc.com/hamm/energy-dispersive-x-ray-spectroscopyeds/>. [Accessed: 02-May-2019].
- [29] Z. Zhong and X. Wang, “Thermal transport in nanocrystalline materials,” *Journal of Applied Physics*, vol. 100, no. 4, Aug. 2006.
- [30] H.-K. Lyeo, D. G. Cahill, B.-S. Lee, and J. R. Abelson, “Thermal conductivity of phase-change materials $\text{Ge}_2\text{Sb}_2\text{Te}_5$,” *Applied Physics Letters*, vol. 89, no. 15, Oct. 2016.
- [31] Y. Zheng, Z. Fu, D. Li, and M. Wu, “Effects of Ball Milling Processes on the Microstructure and Rheological Properties of Microcrystalline Cellulose as a Sustainable Polymer Additive,” *Materials*, vol. 11, no. 7, p. 1057, 2018.
- [32] R. A. Dorey, *Ceramic thick films for mems and microdevices*, vol. 1. Place of publication not identified: William Andrew, 2016.